Electronic Supplementary Material (ESI) for RSC Advances.

Supporting Information

Supporting Information for the paper entitled "Effect of Ligands on Characteristics of $(CdSe)_{13}$ Quantum Dot" by Yang Gao, Bo Zhou, Seung-gu Kang, Minsi Xin, Ping Yang, Xing Dai, Zhigang Wang and Ruhong Zhou

Contents

Part 1. The bare $(CdSe)_{13}$-cage structure.

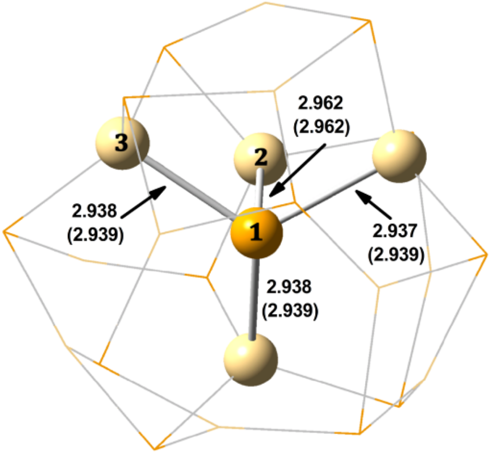

Figure S1. The optimized bare $(CdSe)_{13}$-cage structure. The central Se(1) atom binds with 4 Cd atoms. The arrows point to the corresponding bond lengths with (in parentheses) or without symmetry.

The starting $(CdSe)_{13}$ structure in this study is from the bulk phase wurtzite crystal. After a full structure relaxation, we obtained the lowest energy structure of the bare $(CdSe)_{13}$-cage. Considering that the previous reports had shown that $(CdSe)_{13}$ is C3 symmetric [37], we also studied the bare $(CdSe)_{13}$-cage structure with C3 symmetry. The optimized results showed that the bond length of 2.962Å for Cd(2)-Se(1) at the C3 axis is 0.02Å longer than the other three Cd-Se bond lengths (2.939Å, see Figure S1). Interestingly, it is also consistent with the optimized structure without C3 symmetry. In order to fully understand the stability of Cd(2)-Se(1) bonding, we also tested the structures of the bare $(CdSe)_{13}$-cage bonding with 10 ligands or 1 ligand (with the single ligand placed on the saturated Cd atom). After passivation, the distances between Cd(2) atom and Se(1) atom are 4.241 Å and 4.190 Å, respectively, in the two cases, which are both longer than the normal chemical bonding distance.

Part 2. The dispersion correction of UV UV-vis absorption spectra.

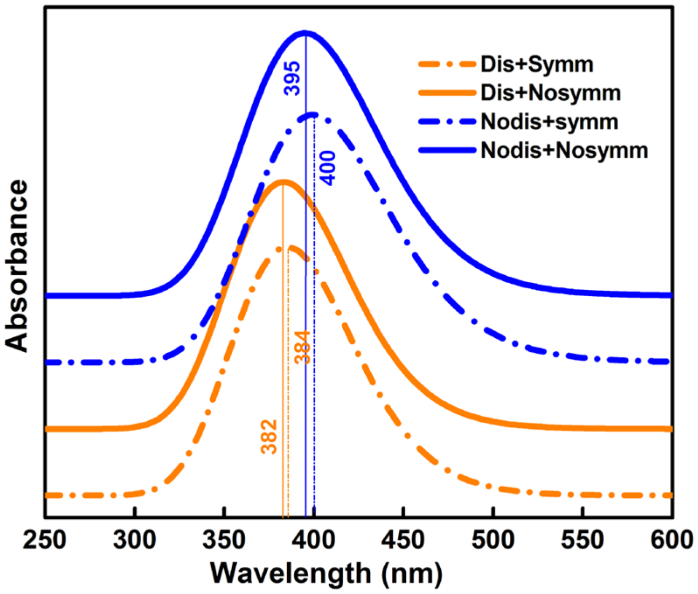

Figure S2. The UV-vis absorption spectra of $(CdSe)_{13}$+9OPMe$_2$-$(CH_2)_2$Me. The blue lines: The geometry optimization results and UV-vis absorption spectra calculated at B3LYP/LANL2DZ level; the yellow lines: The geometry optimization results and UV-vis absorption spectra calculated at B3LYP-D3/LANL2DZ level. Dash-dot lines represent the corresponding structure with C_3 symmetry. The numbers indicate the wavelengths of electronic absorption peaks.

Part 3. The vibrational modes of central QD and the vibrational spectra with different number/length of ligands.

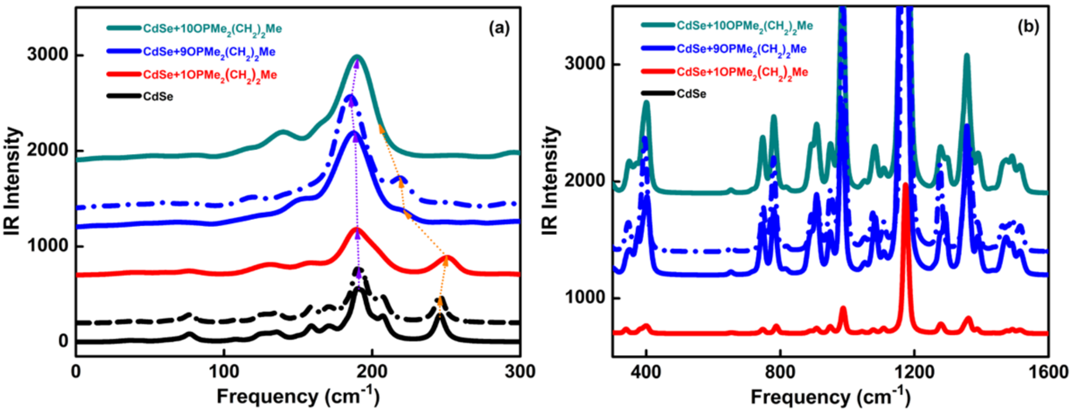

Figure S3. The infrared (IR) spectra of $(CdSe)_{13}+[OPMe_2(CH_2)_2Me]_m$ (m = 0, 1, 9, 10), with (a) showing spectra of the QD at 0-300 cm^{-1}, and (b) showing spectra of the ligands at 400-1600 cm^{-1}. The dash-dot and solid lines represent the corresponding structures with and without symmetries, respectively. The purple and orange dotted lines represent the special position of peaks.

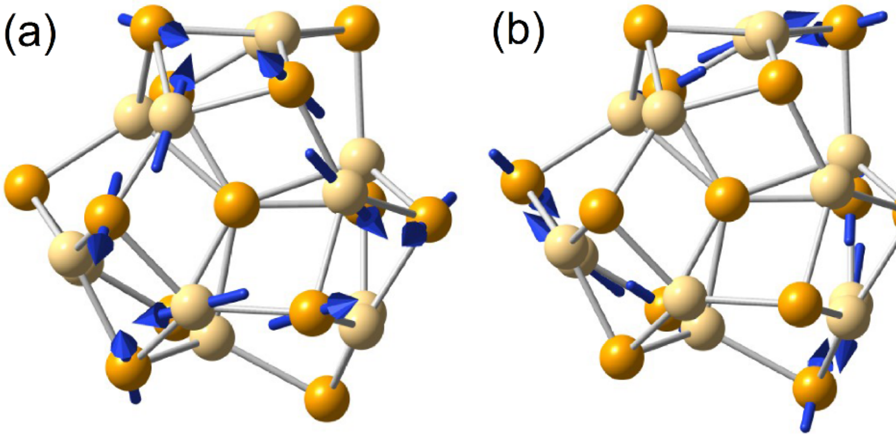

Figure S4. (a) The “twisting mode” of bonds between Cd and Se atoms corresponds to the purple dotted line in Figure S3(a), indicating the lower frequency peak. (b) The “stretching mode” of bonds between Cd and Se atoms corresponds to the orange dotted line, indicating the higher frequency peak in Figure S3(a).

We first observed the ligand effect on internal motions. Figure S3 shows vibrational spectra for the QD core (Figure S3a) and the passivating ligands (Figure S3b). For the bare CdSe core without any organic layer, two major peaks are found at 193.99 cm^{-1} (193.86 cm^{-1}, hereafter data in parenthesis corresponds to the C_3 symmetry) and 246.02 cm^{-1} (245.98 cm^{-1}), respectively (Figure S3a). In our calculations, the symmetry constraint has little effect on the results. The former peak at lower frequency (193.99 cm^{-1}) is assigned as "twisting mode" of bonds among the central Cd and surrounding Se atoms of $(CdSe)_{13}$-cage (Figure S4a). The latter peak at higher frequency (246.02 cm^{-1}) but with relatively lower intensity corresponds to "stretching mode" of the bonds (Figure S4b). Our calculations show that these two vibrational modes are characteristic ("signature peaks"). With the increase of passivation density, their responses are different. The "twisting mode" at the lower frequency is enhanced with the addition of organic molecules even with a slight red shift (i.e., 193.99 (193.86), 192.38, 192.99 (189.35), and 192.05 cm^{-1} from bottom to top), indicating this mode is less sensitive to the surface passivation. On the contrary, the "stretching mode" decreases to almost nil by passivation (i.e., 246.02 (245.98), 248.08，222.87 (218.64), and 205.61 cm^{-1} from bottom to top). This indicates that the stretching motion is more sensitive to the organic layer and dampens to zero by the addition of saturated organic layer.

As another perspective, Figure S3b shows IR spectra of passivating ligand molecules. With regard to the passivation density, no noticeable IR peak shifts was observed for the organic molecules except for the intensity increase. Likewise, the C_3 symmetry gives a negligible effect on the spectra. This indicates that there is little effect on the internal motion of the ligand molecules by coordination on the CdSe surface.

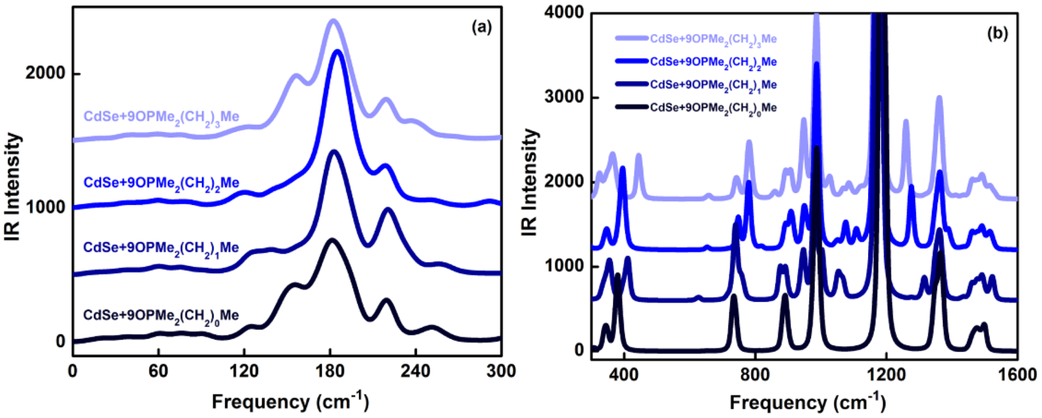

Figure S5. The IR spectra of $(CdSe)_{13}$+9OPMe$_2$(CH$_2$)$_n$Me (n= 0,1-3) with C_3 symmetry. Different colors represent different structures.

In addition to the passivation density, we examined a structural variation of ligand on the vibrational spectra (Figure S5). Based on $(CdSe)_{13}$+9OPMe$_2$(CH$_2$)$_n$Me (n=0, 1-3) with C_3 symmetry, there seem to have no obvious spectral changes in both QD core and ligands by the chain length variation. It is important to maintain a reasonable stability on QD for its desired function, which is also relevant to its cytotoxicity in biomedical applications. These IR vibrational spectra data support that the QD core is stable with only relatively weak coupling to the passivating organic molecules.

Part 4. Comparison of our calculated results with previous reports.

Table S1. The dependence of the maximum excitation wavelength (λ in nm) in UV-vis spectra of CdSe nanoparticles saturated in TOPO solvent on their size (diameter in nm). "Ref" pointed out that the source of the data.

Size (nm)	Ligand	λ(nm)	Ref
0.9	TOPO	400	This work
1.2	TOPO	415	12
1.6	TOPO	445	12 and 64
2.13	TOPO	478	65
2.22	TOPO	490	65
2.4	TOPO	516	66
2.6	TOPO	526	66
2.7	TOPO	534	66
2.9	TOPO	542	66
3.1	TOPO	550	66

Table S1 shows the dependence of the maximum excitation wavelength (λ in nm, "peak position") of CdSe nanoparticles saturated in TOPO solvent on their size (diameter in nm). Previous UV-vis spectra (ref [S1]) also show that the error in the peak position of CdSe QDs increases with the decrease of the size. Furthermore, previous reports indicate that the peak position has a greater uncertainty for QDs with a smaller size due to its larger specific surface area. For these reasons, previous studies mainly focus on those CdSe QDs with sizes larger than 3.0 nm (see ref [S2] for example). Once above this size, the peak position tends to be stable [ref [S3], 66]. Meanwhile, the ligand passivation will generate a clear blue-shift in the UV-vis excitation lights of CdSe nanoparticles [56, 67].

Table S2. The maximum excitation light wavelength (peak position) in UV-vis spectra and the HOMO-LUMO gap of different structures.

Size (nm)	Structure	λ (nm)	Gap (eV)
0.9	$(CdSe)_{13}$	487	3.06
0.9	$(CdSe)_{13}$-symmetry	487	3.06
0.9	$(CdSe)_{13}$+1$OPMe_2(CH_2)_2Me$	495	3.00
0.9	$(CdSe)_{13}$+9$OPMe_2(CH_2)_2Me$	395	3.56

0.9	$(CdSe)_{13}$+9$OPMe_2(CH_2)_2$Me-symmetry	400	3.48
0.9	$(CdSe)_{13}$+10$OPMe_2(CH_2)_2$Me	392	3.66
0.9	$(CdSe)_{13}$+9$OPMe_2(CH_2)_0$Me-symmetry	400	3.48
0.9	$(CdSe)_{13}$+9$OPMe_2(CH_2)_1$Me-symmetry	400	3.48
0.9	$(CdSe)_{13}$+9OPMe2$(CH_2)_2$Me-symmetry	400	3.48
0.9	$(CdSe)_{13}$+9$OPMe_2(CH_2)_3$Me-symmetry	400	3.48

From Table S2, it is obvious that the presence of ligands can shift (blue-shift) the position of the absorption peak, with the largest shift about 95 nm. Once the number of ligands is saturated, the absorption peak only shifts slightly (about a few nms). These results show that the system has apparently reached a “saturated state” with 9 ligands.

Part 5. The excitation energies, oscillator strengths and corresponding molecular orbital compositions of QDs.

Table S3. The excitation energies (E in eV), excitation wavelength (λ in nm), oscillator strengths (f>0), and excited-state composition with contribution percentages [similar statistical methods have been reported in ref 68-70] of the six kinds of structure. The data in the parentheses are referred to the structure with C_3 symmetry.

Structure	E	λ	f	Transition
$(CdSe)_{13}$	2.52 (2.52)	493 (493)	0.032 (0.032)	49% HOMO-2 [Cd 5p 5%, Se 4p 95%] →LUMO [Cd 5s 70%, Se 4p 30%] 49% (HOMO-2 [Cd 5p 5%, Se 4p 95%] →LUMO [Cd 5s 71%, Se 4p 29%])
	2.56 (2.56)	485 (485)	0.030 (0.030)	1% HOMO-1 [Cd 5p 8%, Se 4p 92%] →LUMO 26% (HOMO-1 [Cd 5p 8%, Se 4p 92%] →LUMO) 47% HOMO [Cd 5p 8%, Se 4p 92%] →LUMO 22% (HOMO [Cd 5p 8%, Se 4p 92%] →LUMO)
	2.56 (2.56)	485 (485)	0.030 (0.030)	47% HOMO-1→LUMO 22%(HOMO-1→LUMO) 1% HOMO→LUMO 26% (HOMO→LUMO)
$(CdSe)_{13}$ $+1OPMe_2$ $(CH_2)_2Me$	2.49	498	0.037	3% HOMO-3 [Cd 5p 9%, Se 4p 91%] →LUMO [Cd 5s 69%, Se 4p 31%] 17% HOMO-2 [Cd 5p 7%, Se 4p 93%] →LUMO 22%HOMO-1 [Cd 5p 7%, Se 4p 93%] →LUMO 7%HOMO [Cd 5p 5%, Se 4p 95%] →LUMO
	2.51	495	0.026	8%HOMO-1→LUMO 40%HOMO→LUMO
	2.52	493	0.027	29%HOMO-2→LUMO 18% HOMO-1→LUMO 1%HOMO→LUMO
$(CdSe)_{13}$ $+9OPMe_2$ $(CH_2)_2Me$	3.02 (2.94)	411 (422)	0.085 (0.065)	49% HOMO [Cd 5p 6%, Se 4p 94%] →LUMO [Cd 5s 68%, Se 4p 32%] 49% (HOMO [Cd 5p 5%, Se 4p 95%] →LUMO [Cd 5s 68%, Se 4p 32%])
	3.13 (3.14)	396 (394)	0.096 (0.111)	48% HOMO-1 [Cd 5p 7%, Se 4p 93%] →LUMO 24% (HOMO-2 [Cd 5p 8%, Se 4p 92%]

				→LUMO) 24%(HOMO-1 [Cd 5p 8%, Se 4p 92%] →LUMO)
	3.23 (3.14)	384 (394)	0.125 (0.111)	2% HOMO-3 [Cd 5p 9%, Se 4p 91%] →LUMO 24% (HOMO-2→LUMO) 46% HOMO-2 [Cd 5p 8%, Se 4p 92%] →LUMO 24% (HOMO-1→LUMO)
$(CdSe)_{13}$ $+10OPMe_2(CH_2)_2Me$	3.14	394	0.104	1% HOMO-2 [Cd 5p 8%, Se 4p 92%] →LUMO [Cd 5s 67%, Se 4p 33%] 32% HOMO-1 [Cd 5p 7%, Se 4p 93%] →LUMO 15% HOMO [Cd 5p 8%, Se 4p 92%] →LUMO
	3.16	393	0.117	1% HOMO-2→LUMO 14% HOMO-1→LUMO 34% HOMO→LUMO
	3.18	390	0.122	46% HOMO-2→LUMO 3% HOMO-1→LUMO

In order to further understand the source of electronic absorption peaks, we summarized the excitation energies, oscillator strengths and excited-state composition with contribution percentages in detail in Table S3.

Part 6. Molecular valence orbitals of $(CdSe)_{13}$ with ligands.

Table S4. The highest occupied molecular orbital (HOMO) and the lowest unoccupied molecular orbital (LUMO) of the bare $(CdSe)_{13}$-cage structure, $(CdSe)_{13}$+1$OPMe_2(CH_2)_2Me$, $(CdSe)_{13}$+9$OPMe_2(CH_2)_nMe$ [n=0,1-3] symmetric structure.

Structure	HOMO	LUMO
$(CdSe)_{13}$	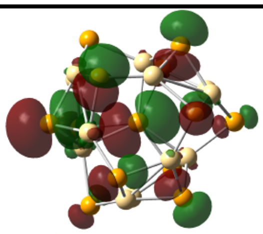	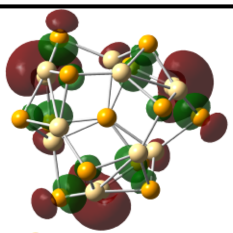
$(CdSe)_{13}$ +1$OPMe_2(CH_2)_2$ Me	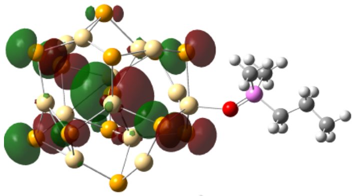	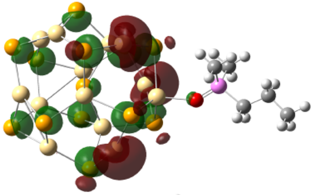
$(CdSe)_{13}$ +9$OPMe_2(CH_2)_0$ Me	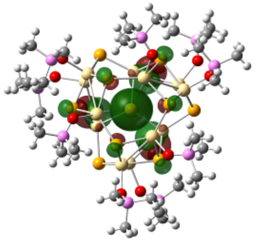	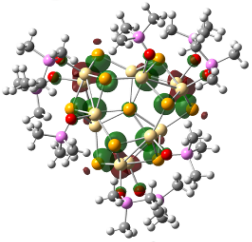
$(CdSe)_{13}$ +9$OPMe_2(CH_2)_1$ Me	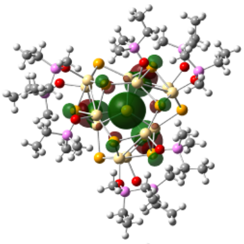	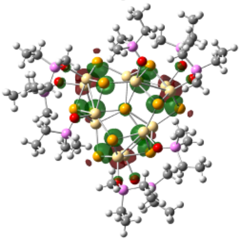
$(CdSe)_{13}$ +9$OPMe_2(CH_2)_2$ Me	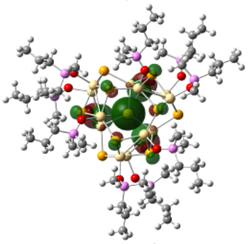	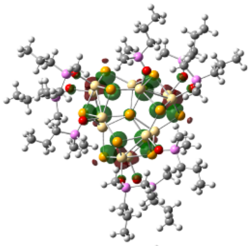
$(CdSe)_{13}$ +9$OPMe_2(CH_2)_3$ Me	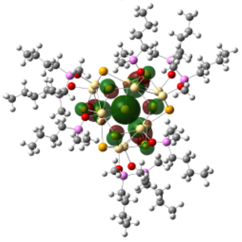	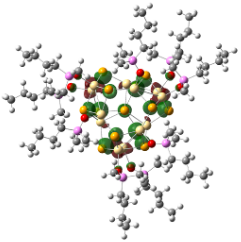

Part 7. Contour maps of charge density deformation in the local area of Cd and O atoms.

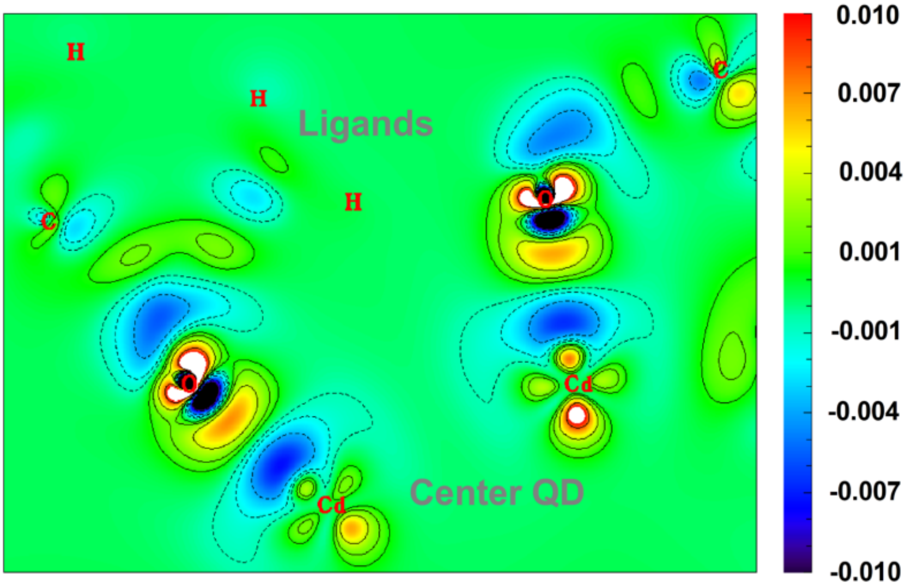

Figure S6. Contour maps of charge density deformation in the local area of Cd and O atoms. The lower right represents the center QD, the upper left represents the ligands. The charge density deformation analysis is performed using the multiWFN code (see ref [S4]).

Part 8. The average binding energy E_b for per ligand molecule between the ligands and the $(CdSe)_{13}$ clusters.

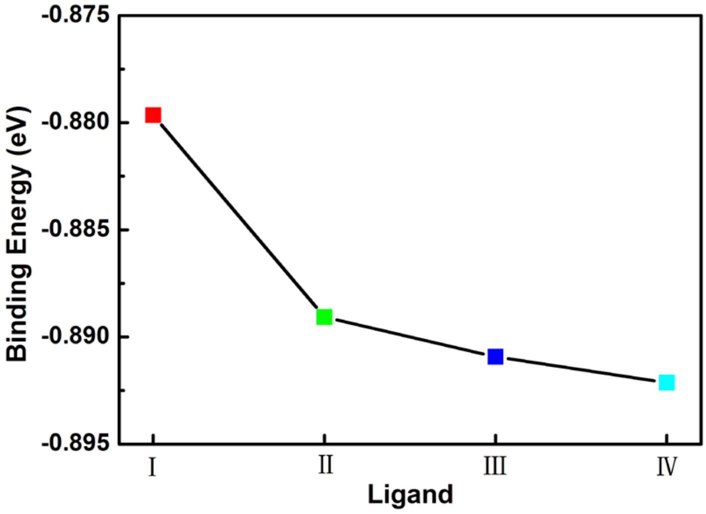

Figure S7. The average binding energy E_b per ligand molecule between the ligands and the $(CdSe)_{13}$ nanoclusters. The abscissa I, II, III, and IV represents $(CdSe)_{13}$+$9OPMe_2(CH_2)_nMe$ (n=0, 1-3) structures for n=0, 1-3, respectively.

Part 9. References for the Supporting Information

S1. W. W. Yu, L. Qu, W. Guo, X. G. Peng, *Chem. Mater*. 2003, **15,** 2854-2860.

S2. M. S. Kang, S. Ayaskanta, D. J. Norris, C. D. Frisbie, *Nano Lett*. 2010, **10,** 3727–3732.

S3. C. M. Donega, S. G. Hickey, S. F. Wuister, D. Vanmaekelbergh, D. Meijerink, *J. Phys. Chem. B.* 2003, **107,** 489-496

S4. T. Lu, F. Chen, *J. Comput. Chem*. 2012, **33,** 580-590.